Results in Engineering 25 (2025) 104118

Contents lists available at ScienceDirect

Results in Engineering

journal homepage: www.sciencedirect.com/journal/results-in-engineering

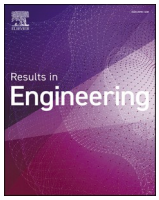

Research paper

Heat transfer analysis of premixed low calorific value landfill gas impinging flame under oxygen and hydrogen enrichment

Kangdong Chen, Udaya Kahangamage *, Kang Tan, Chun-wah Leung

School of Professional Education and Executive Development, The Hong Kong Polytechnic University, Hong Kong

ARTICLE INFO

Keywords:
Low calorific value landfill gas
Impinging flame
Field synergy principle
Heat transfer enhancement

ABSTRACT

The effective utilization of low-calorific value gases is important for meeting growing demand of energy and also addressing associated environmental concerns. In this study, the heat transfer of impinging flames of low-calorific value landfill gas (BG_{30}) was analyzed under hydrogen and oxygen enrichment. Numerical simulations were conducted to estimate the heat transfer from the impinging flames and compared with that of the high-calorific value landfill gas (BG_{60}) flames. The heat flux from the impinging flame was analyzed from the perspectives of Laminar Burning Velocity (LBV), temperature and velocity fields of the impinging flame using the field synergy principle. The heat transfer from impinging flame on to the target plate was categorized into heat transfer from the heat generated in the boundary layer (Q_ϕ) and convective heat transfer (Q_s). The results demonstrate that BG_{30}, after being enriched with 29% hydrogen and 39% oxygen, exhibits an LBV equivalent to that of BG_{60}. The optimal convective heat transfer is achieved when the target plate is positioned slightly above the tip of the flame cone, while the optimal total heat transfer occurs when the target plate is located approximately 2/3 of the flame cone height. Based on the insights from numerical investigations, a cap-shaped target plate was tested for heat transfer from impinging flames. It effectively enhanced the total heat transfer rate on to the target plate.

1. Introduction

There are various alternative energy sources that are being explored to face the current and future challenges of energy supply [1–3]. Among them, some of the combustible gases such as landfill gas, producer gas, coal gas, blast furnace gas, etc. are categorized as lean gases due to low energy content. However, as energy sources, they are becoming attractive for some applications due to considerably lower cost and availability in large volumes. Direct combustion of these gases for heat recovery is very challenging due to the presence of a large percentage of inert gases, difficulty in maintaining stable flame, undesirable emissions and low energy output. It also requires a large volume of gas to produce equivalent energy output that can be obtained from traditional fuels such as natural gas. Fuel enrichment technique has been successfully used to overcome some of the challenges associated with lean gases and used for various energy applications such as supplementary fuel for industrial boilers [4], process heating [5], greenhouse heating [6], processing of landfill leachate [7], etc.

There are various research studies on lean gases [8–12] covering topics such as combustion and flame structures [8–10], heat transfer characteristics [11] and pollution emissions [12]. Since lean gases are mainly used for heating applications with the use of impinging flames, the flame-wall heat transfer process is very important to enhance the heat recovery process. There are limited investigations specifically focusing on premixed impinging flame of low calorific value gases. Therefore, the focus of this research study is to investigate the flame-wall heat transfer characteristics of impinging flame with low calorific value landfill gas (LCV LFG) under the hydrogen-rich and oxygen-rich conditions.

When working with low-grade energy sources, it is important to employ fuel enrichment techniques and pay attention to the heat transfer enhancement methods to effectively convert available limited amount of chemical energy into useful heat energy. It is also important to reduce the loss of energy during heat transfer process in general [13]. In impinging flames, convective heat transfer plays an important role. Focusing on convective heat transfer, Guo et al. [14,15] proposed and validated the field synergy principle to enhance heat transfer. The field synergy principle emphasizes the significant impact of the temperature field, velocity field and their synergy on heat transfer enhancement. According to this principle, the better the synergy between velocity of the fluid flow and the temperature gradient, the more effective the heat

* Corresponding author.
E-mail address: udaya.kahangamage@cpce-polyu.edu.hk (U. Kahangamage).

https://doi.org/10.1016/j.rineng.2025.104118
Received 6 November 2024; Received in revised form 9 December 2024; Accepted 20 January 2025
Available online 21 January 2025

Nomenclature

ρ	gas density, kg/m^3
C_p	specific heat at constant pressure, J/ (kg·K)
u_s	flow velocity in x direction, m/s
LBV	laminar burning velocity, cm/s
θ	angle between axis of flame and flame front, rad
T	temperature, K
P	pressure, Pa
λ	thermal conductivity, W/(m·K)
φ	equivalence ratio
H	nozzle-to-plate distance, mm
h	flame cone height, mm
r	radial distance from axis of flame, mm
z	axial distance from the burner nozzle, mm
$\overline{U}$	flow velocity vector, m/s
$\overline{\nabla T}$	temperature gradient, K
β	synergy angle, rad
Q_w	total heat transfer rate, W
Q_Φ	heat generated in boundary layer due to combustion, W
Q_s	heat entering boundary layer due to convection, W

transfer is between the fluid and the solid target. However, the original concept of field synergy principle presented by Guo et al. does not contain the effect of internal heat sources, leading to a lack of interest among scholars in the field of combustion to adapt this principle to study heat transfer. It was only when researchers encountered bottlenecks in micro-scale combustion studies that they began to seek breakthroughs based on the field synergy principle. Jiaqiang et al. [16] investigated field synergetic degree of the premixed methane/air combustion in a micro two-steps combustors. In their investigations into wall-flow and heat transfer characteristics within diesel particulate filters [17], they discovered that variations in inlet pressure alter the angle formed between the velocity vector and the temperature gradient. Consequently, the variation of the inlet pressure results in changes to the degree of synergy exhibited by the velocity and temperature fields. Jiaqiang et al. [18] also conducted a field synergy analysis on the temperature gradient and velocity vector under different inlet velocities of hydrogen-air combustion. They demonstrated that, with constant inlet velocity of air, a decrease in the inlet velocity of hydrogen can significantly improve combustion stability, which will contribute to stabilizing non-premixed combustion in micro-combustion chambers. Fu at al. [3] studied the relationship between the synergistic effect of velocity-temperature field and thermal NO_x generation. Fu et al. [19] also discovered that when the hydrogen content surpasses 20% by volume, the introduction of hydrogen significantly influences the field synergy within the combustor. This is advantageous for achieving a more uniform temperature distribution at the exit, while also maintaining a relatively low flow resistance. Tan et al. [20] conducted a study on the distribution of synergy angle β and the level of synergy within a rearward-step micro combustor. They observed that in the stepped structure of the burner, at an inlet velocity of 7.0 m/s and an equivalence ratio of 1.5, the three-step micro-combustion chamber achieved a maximum synergy degree of 2.99%, which significantly enhanced the average outer wall temperature of the micro-combustion chamber. Liu et al [21] observed that increasing the secondary oxygen ratios from 0% to 40% in a fuel comprising 75% hydrogen and 25% nitrogen resulted in a significant improvement in the synergy angle β on the central plane.

It is evident that the current field synergy analysis in the field of combustion is mostly applied to the analysis of micro-scale combustion, and few of these studies explicitly distinguished the internal heat generation due to chemical reactions within the flow and convective heat transfer in combustion process [22]. Incorporation of the effect of internal heat generation is important for heat transfer analysis of combustion as internal heat generation by chemical reactions is a core issue of combustion. Wei et al. [23] discussed the synergistic effect of temperature and velocity fields on heat transfer in blended methane-hydrogen impingement flames. Raj et al. [24] observed that the thermal image averages reveal the presence of an envelope (known as the thermal boundary layer) adjacent to the impingement surface, which significantly impacts on heat transfer at the target plate. In our previous work [22], we have considered the impacts of heat generation within the boundary layer and convective heat transfer on the heat transfer to the target plate, and conducted a detailed analysis of the heat transfer characteristics of both premixed and diffusion flames of biogas. This paper delves into the heat transfer due to heat generation in the boundary layer and convective heat transfer associated with a single flame colliding with a wall, thereby explaining the causes of local heat flux on the heated wall surface. Furthermore, from a novel perspective of field synergy principle, it reveals the contributing factors on heat transfer characteristics of impinging flames of low calorific value landfill gases with hydrogen enrichment and oxygen enrichment.

2. Methodology

For numerical investigations, ANSYS Chemkin-Pro and Fluent with GRI-Mech 3.0 reaction mechanism were used in this study. The objective was to investigate the heat transfer performance of hydrogen and Oxygen-enriched low calorific value LFG by studying laminar burning velocity (LBV), adiabatic flame temperature and heat flux of premixed impinging flames of various fuel mixtures. A gas mixture of 30 vol% CH_4 and 70 vol% CO_2 (BG_{30}) was used in this study to represent the low calorific value LFG and the premixed flame model was adopted.

2.1. Modelling with ANSYS Chemkin-Pro

To investigate the LBV of flames, Chemical and Phase Equilibrium (0-D) and Laminar Flame-Speed model (1-D) were adopted. Wherein, the solver of the 1-D model is developed as Premix code by Chemkin. The Multicomponent transport and thermal diffusion (Soret Effect) were incorporated in the reactor model. The typical laminar premixed Bunsen burner flame studied has been simplified from three-dimensional to two-dimensional axisymmetric model shown in Fig. 1(a). In the two-dimensional model, it was assumed that the radial velocity v in the r direction (Fig. 1(b)) changes linearly along radial direction. It allows the 2-D flow analysis to be simplified into 1-D analysis in Chemkin [25,26].

2.2. Modelling with ANSYSY Fluent

The 2-D premixed flame model built in ANSYS Fluent is shown in Fig. 1(b), and only half of it is meshed. To provide a clearer view of the grid encryption area, Fig. 1(b) displays a larger grid size, whereas smaller grids are used in the actual calculations. Further details on

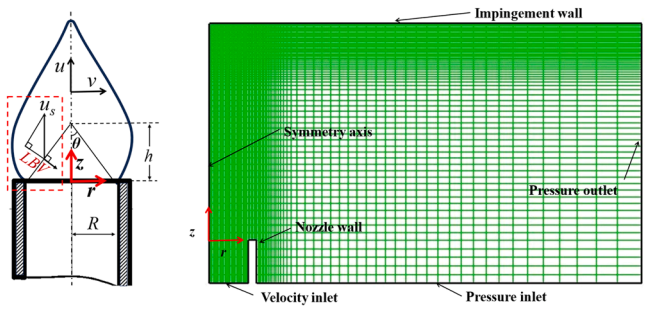

Fig. 1. Sketches of the numerical domains.

model development and grid size are provided in Ref [22]. A quadrilateral structured grid is used. The fuel-air mixture is supplied into reaction domain through a circular tube with a diameter of 9 mm. The specified boundary conditions such as velocity-inlet, pressure-inlet, pressure-outlet, symmetry axis, and no-slip aluminum nozzle wall are shown in Fig. 1(b). The SST k-omega turbulent model, laminar finite-rate model, and P1 radiation model were adopted in this study. The three fundamental conservation Eq.s must also be discretized and solved.

Continuity Eq.:

$$\frac{\partial \rho}{\partial t} + \frac{\partial}{\partial x_i}(\rho u_i) = 0 \tag{1}$$

Where, x_i represents the Cartesian coordinate system, and u_i represents the velocity components on the coordinate system.

Momentum Eq.:

$$\frac{\partial}{\partial t}(\rho u_i) + \frac{\partial}{\partial x_i}(\rho u_i u_j) = -\frac{\partial p}{\partial x_i} + \frac{\partial \tau_{ij}}{\partial x_i} + \rho f_i \tag{2}$$

Where, the external force on the fluid element is f_i = -g, when the fluid element is only subjected to gravity.

Energy Eq.:

$$\frac{\partial \rho H_e}{\partial t} + \nabla(\rho H_e u_i) = \frac{\partial p}{\partial t} + u_i \frac{\partial p}{\partial x_i} + \tau_{ij}\frac{\partial u_i}{\partial x_j} + \dot{\phi} \tag{3}$$

Where, H_e represents enthalpy ($J{\cdot}kg^{-1}$); Φ represents energy source ($W{\cdot}m^{-3}$), which in this context denotes the heat of combustion generated through chemical reactions.

2.3. Grid Independence Verification

The number of nodes of the grid in the overall calculation area changed from 17,940 to 78,000 to verify grid independence, and the results are shown in Fig. 2 (BG_{60}-air flame is used for this verification study). The heat flux in grids 2 and 3 is nearly identical. Therefore, in order to conserve computational resources, grid 2 is chosen as the computational grid for this study.

2.4. Field Synergy Principle

The energy Eq. for laminar flow within a two-dimensional boundary layer on the wall is:

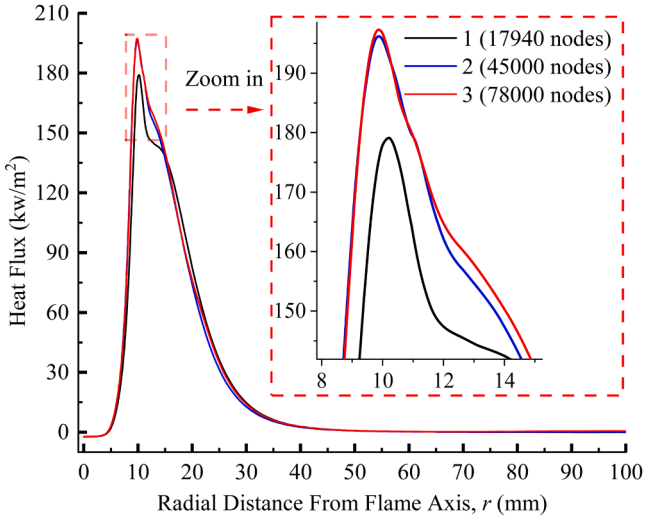

Fig. 2. Effect of grid size on radial heat flux of BG_{60}-air flame distribution at the impingement plate surface.

$$\rho C_p\left(u\frac{\partial T}{\partial x} + v\frac{\partial T}{\partial y}\right) = \frac{\partial}{\partial y}\left(\lambda\frac{\partial T}{\partial y}\right) \tag{4}$$

where: ρ is fluid density, Cp is specific heat at constant pressure, u and v are flow velocities, T is fluid temperature and λ is thermal conductivity.

Guo et al. [27] represented the convection term in Eq. (4) as the dot product of velocity and temperature gradients as follows:

$$u\frac{\partial T}{\partial x} + v\frac{\partial T}{\partial y} = \overline{\boldsymbol{U}}\cdot\overline{\nabla \boldsymbol{T}} = |\overline{\boldsymbol{U}}||\overline{\nabla \boldsymbol{T}}|\cos\beta \tag{5}$$

where β is the synergy angle between flow velocity vector and temperature gradient.

Prior research studies have shown that the factors affecting convective heat transfer are not only temperature and flow velocity, but also the synergy angle [28]. For flame impingement heat transfer, it is also necessary to consider the thermochemical heat release at the target plate boundary layer. Therefore, in our previous work [22], the heat transfer of impinging flames was divided into two parts; namely the heat generation in the boundary layer of the wall surface (Q_Φ) and the convective heat transmitted to the boundary layer (Q_s), as shown in Fig. 3.

Fig. 3 illustrates several key terms associated with the analysis of the field synergy principle in section 4.5 of this paper: target plate, heat generation in the boundary layer (Q_Φ), convective heat transfer (Q_s), total heat transfer rate (Q_w), velocity vector, temperature gradient, and synergy angle (β). Additionally, Table 1 provides the details of the gas mixtures used in this study.

3. Simulation Validation

3.1. 1D Model Validation in ANSYS Chemkin-Pro

Fig. 4 shows the experimental [29] and computational LBV of BG_{50} and H_2-enriched BG_{50} flames at 0.1Mpa and 300 K. The opened and closed symbols in Fig. 4 represent the experimental and simulation data for LBV, respectively. With the use of ANSYS Chemkin-Pro with GRI-Mech 3.0, the LBV of BG_{50} (CH_4-50% + CO_2-50%) with 0% and 40% H_2 enrichment (R_H=0.0 and R_H=0.4) were studied computationally. The numerical results obtained are in better agreement with the experimental data reported by Yadav et al. [29].

3.2. 2D Model Validation in ANSYS Fluent

In the current study, it is expected to perform numerical study of the flame structure of hydrogen-enriched and oxygen-enriched low calorific value LFG using GRI-Mech 3.0 mechanism in ANSYS Fluent. For the validation study, computational models for BG_{60}-air and BG_{60}/hydrogen-air fuel mixtures are used and results are compared with experimental data available in reference [30].

Fig. 5 shows a comparison of flame height obtained from numerical simulations of BG_{60}-air and BG_{60}/hydrogen-air mixtures with corresponding experimental results presented in reference [30]. Each premixed flame, whether experimental or simulated, appears as a stationary flame attached to the burner nozzle. As reported in reference [30], the height of the conical flame front of the pure BG_{60}-air premixed flame is 24 mm, which decreases to 19 mm with the addition of 10% hydrogen. A similar flame behavior is observed in the simulation study as shown in Fig. 5. Therefore, it is evident that the computational results of BG_{60}/hydrogen-air mixtures developed with the use of GRI-Mech 3.0 mechanism is in good agreement with the experimental results obtained by Zhen et al. [30]. The effectiveness of using GRI-Mech 3.0 mechanism in simulating premixed flame structure of low heating value fuel gas mixtures is also reported by Shin et al. [31] through experimental verifications. In addition, to enhance the persuasiveness of the discussion, Figs. 10(a) and 11 below compare the distributions of local heat flux and

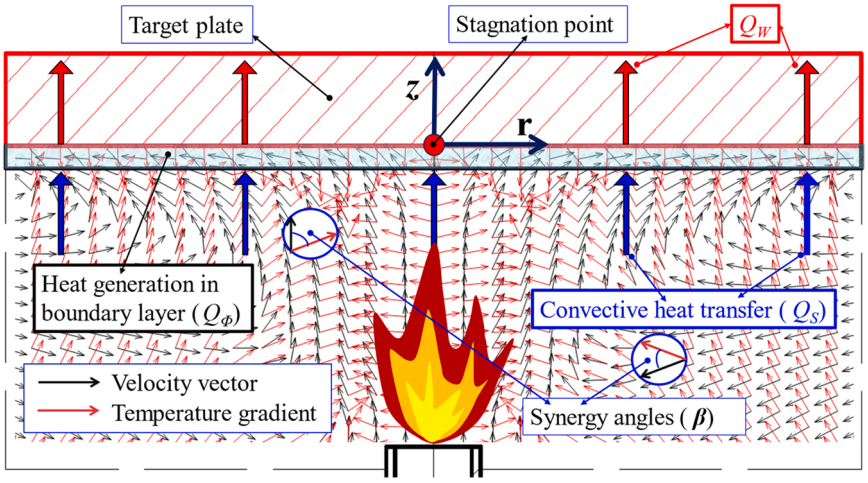

Fig. 3. Illustration of the mode of heat transfer from impinging flame and key terminology.

Table 1
Details of the gas mixtures used.

Designation	Composition of Fuel	O_2 Content in Oxidizer	equivalence ratio ϕ	Input* Energy Q_{in}
BG_{30}	CH_4-30% + CO_2-70%	O_2-21% + N_2-79%	1.2	206 W
BH_{30}	(CH_4-30% + CO_2-70%)-71%+ H_2-29%	O_2-21% + N_2-79%	1.2	217 W
BO_{30}	CH_4-30% + CO_2-70%	O_2-39% + N_2-61%	1.2	305 W
BG_{60}	CH_4-60% + CO_2-40%	O_2-21% + N_2-79%	1.2	241 W

* The energy inputs are calculated for volumetric flowrate of Q = 63.7 cm^3/s.

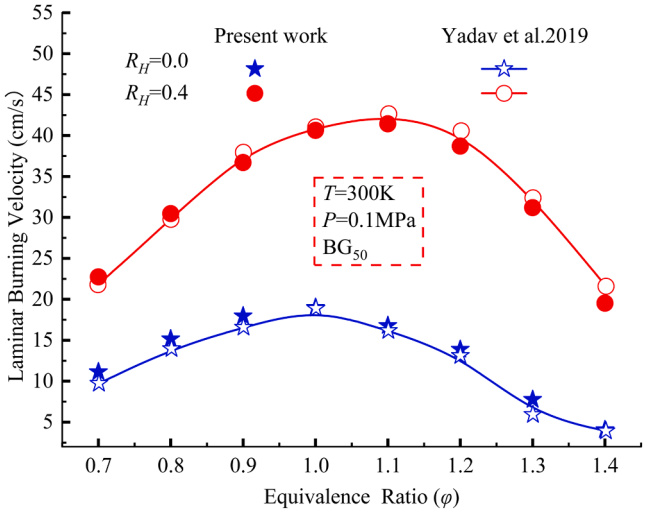

Fig. 4. Comparison of predicted laminar burning velocity of BG_{50}-air and BG_{50} /hydrogen-air mixtures and reference values from literature [29] at ambient conditions (T = 300 K and P = 0.1MPa).

total heat transfer rate, respectively. The trends of variations of the numerical results are consistent with those of the experimental results.

4. Results and Discussion

4.1. Laminar Burning Velocity (LBV)

Laminar burning velocity (LBV) characterizes the spatial movement speed of the flame front during the combustion process and is crucial data for studying flame stability. The LBV is also a significant factor influencing the velocity field of the entire combustion zone that plays a crucial role in heat transfer of impinging flame.

The combustion characteristics of various types of fuels under hydrogen-rich conditions have been extensively discussed in many existing literatures [26,32]. Therefore, the main focus here is to analyze the LBV and adiabatic temperature of BG_{30} fuel gas under oxygen-rich conditions, utilizing the results obtained from Chemkin calculations (BG_{30} with 39% oxygen enrichment is designated as BO_{30}, as given in Table 1).

Fig. 6 illustrates the variation of LBV with change in secondary oxygen content added to BG_{30} at equivalence ratios of φ=0.8, 1.0 and 1.2. It can be seen that as the oxygen concentration in the oxidizer increases, the LBV of BG_{30} also increases linearly. Fig. 6 also demonstrates the variation of adiabatic flame temperature. The adiabatic flame temperature continues to rise with the increase of secondary oxygen content. However, the rate of increase reduces gradually. The main reason why 39% oxygen concentration was selected as the oxidant for oxygen rich combustion in Table 1 is that when φ = 1.2, BO_{30} exhibited almost the same LBV as BG_{60} (as shown in Fig. 7), which facilitates subsequent comparative investigations in this article. Establishing this comparison framework is crucial for facilitating a more intuitive understanding of their respective performances. Similarly, BH_{30} (BG_{30}-71% & H_2-29%) follows the same rationale, as illustrated in Fig. 7.

Fig. 7 exhibits the variation of LBV for four different fuels (BG_{30}, BH_{30}, BO_{30}, and BG_{60}) as the equivalence ratio (φ) ranges from 0.7 to 1.4 in Chemkin. The LBVs initially increase and then decrease within this equivalence ratio range. It is noteworthy that the BH_{30}, BO_{30}, and BG_{60} flames exhibit similar LBVs at an equivalence ratio of 1.2. Therefore, due to their significance in understanding the combustion characteristics of the fuels, they have been selected as the focus of this study.

4.2. Flame Temperature

Fig. 8 illustrates the contours of flame temperature for the BH_{30}, BO_{30}, and BG_{60} impinging flames, obtained from simulations performed

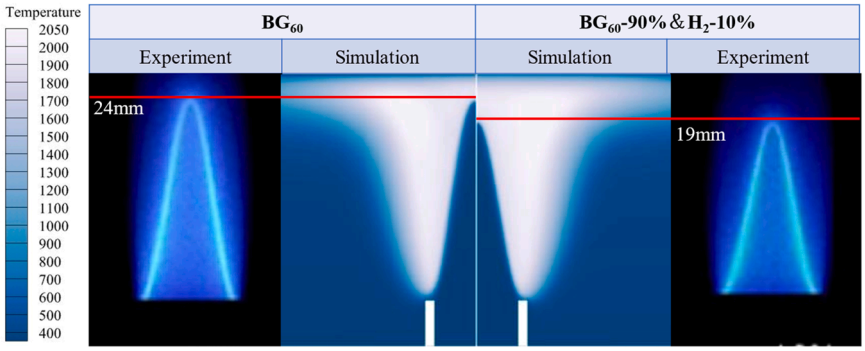

Fig. 5. Comparison of experimental [30] and simulation images of impinging flame.

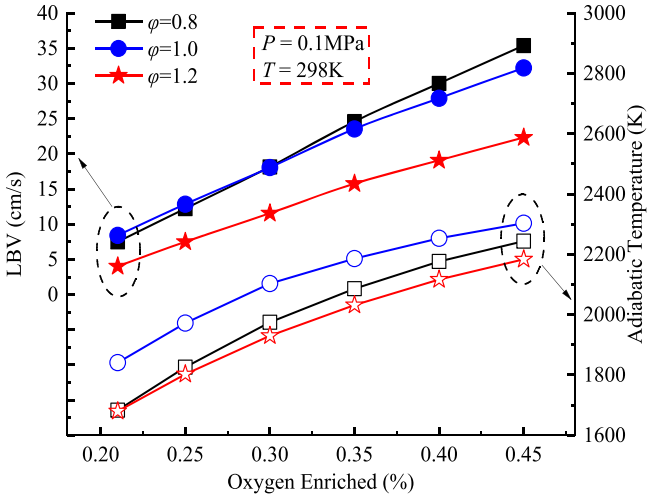

Fig. 6. Variation of LBV and Adiabatic Flame Temperature of BG_{30} with increase in Oxygen fraction added to fuel-air mixtures for various equivalence ratios (φ).

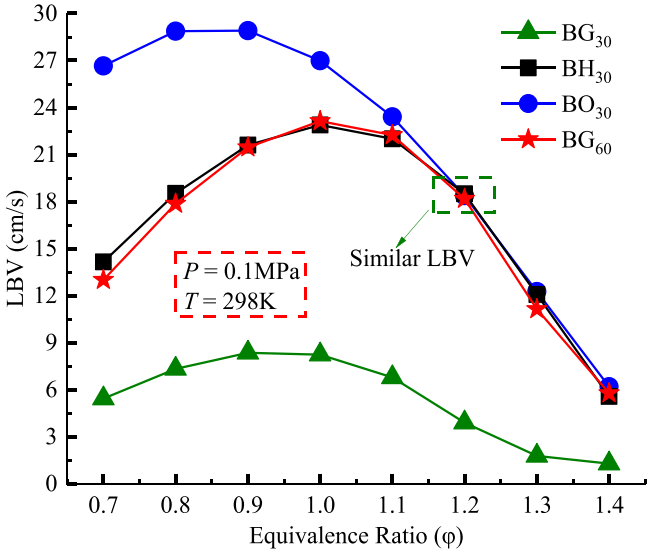

Fig. 7. Variation of LBV of different gas-mixtures with increase in equivalence ratio (φ), at initial temperature 298K and initial pressure 0.1MPa.

using ANSYS Fluent. The Fig. clearly depicts the distinct characteristics of the flame temperature distributions. As observed, the combustion performance of the low calorific value gas BG_{30}, which cannot be stably

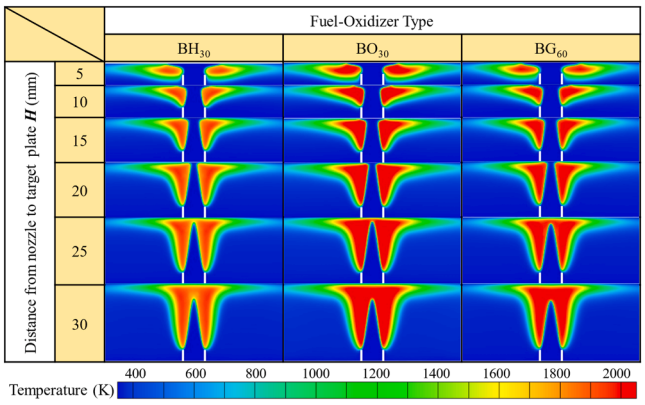

Fig. 8. Temperature contours of BH_{30}, BO_{30}, and BG_{60} impinging flames at different nozzle-to-plate distances ($\varphi = 1.2$).

burned, has been significantly enhanced under hydrogen-rich and oxygen-rich conditions.

The peak temperature of the BG_{60}-air flame at an equivalence ratio of 1.2 is 2040K for the conditions tested, whereas the peak temperature of the BH_{30}-air flame reaches 1910K, and that of the BO_{30}-air flame is even higher, rising to 2143K. This is a significant improvement compared with the peak temperature associated with BG_{30}-air flame which is around 1300K [9]. As the nozzle-to-plate distance (H) increases, the temperatures of the three flames (BH_{30}, BO_{30}, and BG_{60}) continue to rise until the flame cones no longer in contact with the target plate. This is due to the partial suppression of combustion performance as the flame cones touch the target plate. The temperature variations observed among the BH_{30}, BO_{30}, and BG_{60}-air flames are attributed to the distinct chemical energy inputs of their respective fuel gases. As indicated in Table 1, under identical volumetric flow rate conditions of Q = 63.7cm³/s, the input heat powers for BH_{30}, BO_{30} and BG_{60}-air flames are 217W, 305W, and 241W, respectively. This is the primary reason why the flame temperature of BH_{30}-air flame is lower than that of BG_{60}-air flame, while the flame temperature of BO_{30}-air flame is higher than BG_{60}-air flame.

According to the field synergy principle, heat transfer is influenced not only by the temperature field but also by the velocity field and the synergy angle. To provide a detailed understanding of the heat transfer of the impinging flame, a comprehensive explanation has been presented in Section 4.5. In the following sections, the effect of laminar burning velocity, and the flame velocity field on the heat transfer characteristics of impinging flames are discussed.

4.3. *Flame velocity field*

Since BH_{30}, BO_{30} and BG_{60} premixed flames have similar LBV at φ =

1.2, they also have similar flame heights. A comparative analysis of velocity fields of the flames is performed at the same conditions. The analysis revealed both similarities and differences in their velocity fields as depicted in Fig. 9, all of which directly impact the heat transfer efficiency to the target plate. In terms of similarities, all fuels release a large amount of heat after chemical reactions, which leads to an increase in gas temperature and subsequent volume expansion. Therefore, it can be clearly seen that after the flame front, the gas velocity increases significantly, which is beneficial for impingement heat transfer. As the nozzle-to-plate distance increases, the fluid velocity near the plate noticeably decreases, which is unfavorable for heat transfer to the plate from the impinging flame. However, it is not necessarily ideal for the nozzle to be too close to the target plate either. This is because it can cause the fuel to rebound and move away from the plate before undergoing complete combustion. For example, this can occur when the nozzle-to-plate distance (H) is 5mm.

One of the differences is that compared to the other two flames, the magnitudes of velocity contours of the velocity field in the BH_{30} flame are significantly lower, as shown in Fig. 9. This is attributed to different chemical reaction pathways (R1: $2H_2+O_2=2H_2O$ and R2: $CH_4+2O_2=CO_2+2H_2O$). The main reason for the lower velocity of the hydrogen-rich flame (BH_{30}) can be attributed to the fact that the gas undergoing reaction via the R1 pathway results in a reduction of one-third of the molecular quantity compared to the reaction via the R2 pathway. For example, in reaction R1, there are only 2 moles of product ($2H_2O$) out of 3 moles of reactants ($2H_2+O_2$). But in reaction R2, 3 moles of reactants (CH_4+2O_2) still have 3 moles of products (CO_2+2H_2O).

4.4. Impingement Heat Flux

Heat flux, also known as thermal flux or heat-flow density, refers to the amount of heat energy passing through a unit area in a unit time, and it is a directional vector. Fig. 10 shows the heat flux of impinging flames (BH_{30}, BO_{30}, and BG_{60}) which have been calculated using the ANSYS Fluent software. Local heat flux values have been obtained at different radial positions from the central axis of the flame for different nozzle-to-plate distances. Experimental data for the BG_{60} impinging flame available in the literature [30] have been used for verification and comparison of the simulation results.

Fig. 10 (a) presents a comparison between the experimental and simulation data for the local heat flux of the BG_{60}-air impinging flame. It is evident that when r is less than 15mm, the simulation results obtained using Fluent software underestimate the experimental data as reported in the literature [30]. However, within the range of r = 15mm to 30mm, the numerical data align very well with the experimental measurements. This range is critical because the high heat flux values and the large integration area make it the most significant segment of the curve. For r > 30mm, no experimental data are available, and the simulation data

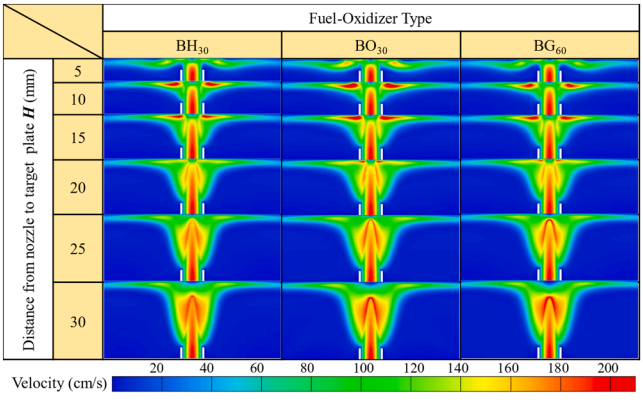

Fig. 9. Velocity contours of BH_{30}, BO_{30} and BG_{60} impinging flames for different nozzle-to-plate distances ($\varphi = 1.2$).

decrease from 30 kW/m^2 to 0. Therefore, the integrals of both datasets are consistent (as shown in Fig. 11), indicating that the numerical results are reliable.

Fig. 10(b) and (c) show the radial distribution of heat flux of BH_{30} and BO_{30} impinging flames compared with BG_{60} flame. It can be seen that due to the different chemical input energy of BH_{30} (217W) and BO_{30} (305W), their radial heat flux distribution is lower and higher than that of BG_{60} (241W), respectively. To determine the total heat transfer rate (Q_w), each heat flux profile in simulation is integrated across a circular region with a radius of 40 mm, following the specified Eq. 6.

$$Q_w = \iint_A \dot{q}_{local} dA = 2\pi \int_0^r \dot{q}_{local} r dr \tag{6}$$

Fig. 11 presents the total heat transfer rates of the three flames: BH_{30}, BO_{30}, and BG_{60}. The experimental data of total heat transfer rates for BG_{60}, as reported in the literature [30], is also incorporated in the Fig.. The comparison of the experimental and simulated total heat transfer rates of BG_{60} shows that the simulated results underestimate the experimental results. However, data values are quite close, and simulation results closely reproduced the shape of the experimental data curve. With the increase of the nozzle-to-plate distance (H), the total heat transfer rates of the three flames first increase and then decrease, reaching a peak at around H=15mm. As indicated in Table 1, the three flames exhibit variations in their chemical input energy, which consequently results in varying total heat transfer rates, as depicted in Fig. 11. Hence, it is not recommended to evaluate the quality of the fuel gas mixtures solely based on a single criterion of total heat transfer rate.

Fig. 12 illustrates the total heat transfer efficiency of the impinging flames. Heat transfer efficiency is calculated by: Q_w/Q_{in}. It can be seen that the low calorific value gas BG_{30}, after enriching with hydrogen (29%) and oxygen (39%), not only has a similar LBV to biogas BG_{60} (for $\varphi = 1.2$), but also has a similar heat transfer efficiency.

It is evident that the heat transfer characteristics are closely related to temperature field (as shown in Fig. 6) and velocity field (as shown in Fig. 9) of the impinging flames. The following section analyzes the heat transfer characteristics of impinging flames from a new perspective of the field synergy principle, by considering the flame temperature field, velocity field, and the synergy angle between the two. By utilizing the field synergy principle, a clearer understanding of the heat transfer characteristics of impinging flames can be achieved. It is crucial to recognize that the heat transfer of impinging flames predominantly involves convective heat transfer, along with thermochemical heat release by the burning fuel within the boundary layer of the heated wall.

4.5. Use of Field Synergy Principle to Analyze Heat Transfer Characteristics

Fig. 13(a) and (b) show the field synergy analysis of heat transfer for the BH_{30} and BO_{30} impinging flames at different nozzle-to-plate distances, respectively. It can be observed that convective heat transfer rate (Q_s) first increases, then tends to plateau at H=25mm, and gradually decreases thereafter. The evaluation index S_t as defined in ref. [22] is positively correlated with Q_s, indicating that the field synergy principle can be used to predict the heat transfer performance of impinging flames.

It is evident that heat generation in the boundary layer (Q_Φ) gradually decreases as H increases due to the reduction of fuel mole fraction near the target plate as shown in Fig. 14(a) which shows contours of the fuel mole fraction.

The convective heat transfer (Q_s) shows an increasing trend with the increase of H. When H is higher than the flame cone height, it tends to flatten and then begins to decrease. Fig. 14(b) shows the trend of Q_s variation with H for three types of flames: BH_{30}, BO_{30}, and BG_{60}, and also provides temperature contours and velocity vector contours. According to the field synergy principle, convective heat transfer is

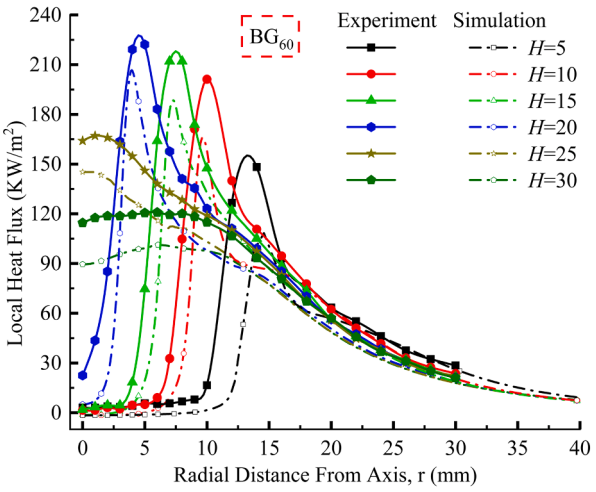

(a) Experimental [30] and numerical data of BG_{60} for verification of simulation data.

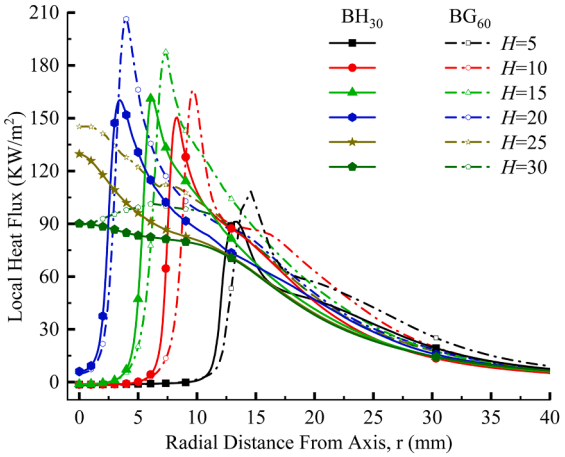

(b) Numerical data of BH_{30} and BG_{60}

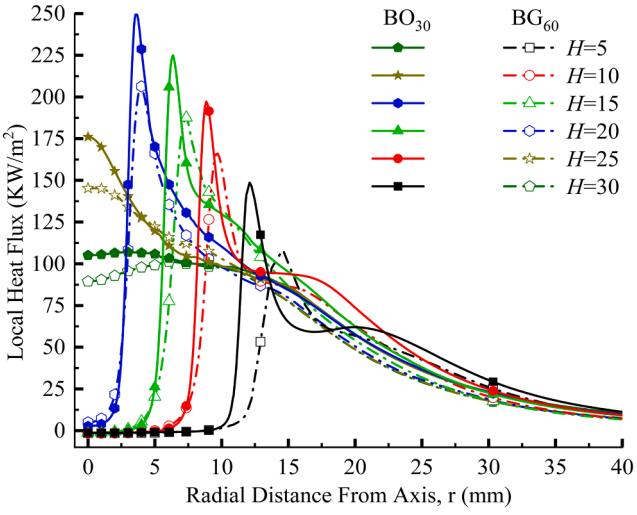

(c) Numerical data of BO_{30} and BG_{60}

Fig. 10. Comparison of local heat fluxes of the different flames at $\varphi = 1.2$ for H = 5-30 mm. (a) Experimental [30] and numerical data of BG_{60} for verification of simulation data. (b) Numerical data of BH_{30} and BG_{60}, (c) Numerical data of BO_{30} and BG_{60}.

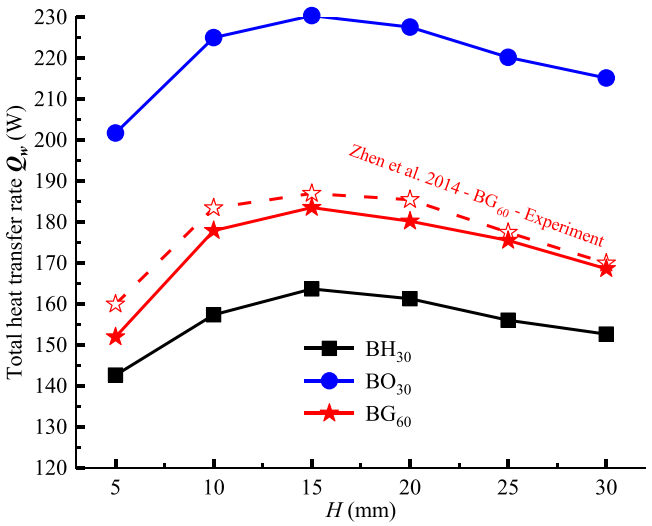

Fig. 11. Total heat transfer rates of the premixed impinging flames at different nozzle-to-plate distances for BG_{60}, BO_{30} and BH_{30}.

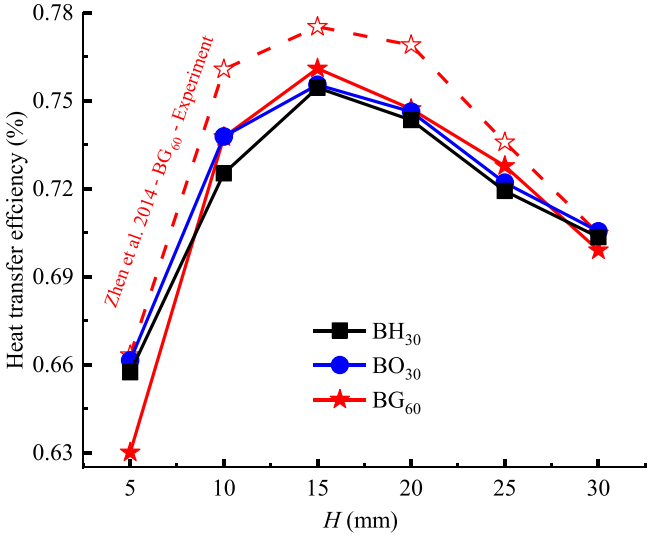

Fig. 12. Heat transfer efficiency of BG_{60}, BO_{30} and BH_{30} at $\varphi = 1.2$.

determined by the temperature field, velocity field, and the synergy angle between the two.

As shown in Fig. 14(b), when H is less than the flame height, the flame temperature is relatively low (about 1600K to 1700K), and the synergy angles β is not optimal (near right angle where heat transfer is the worst). Consequently, the evaluation index S_t is low, resulting in lower Q_s. However, when H is approximately equal to the flame height, the peak temperature appears near the target plate, and the unburned cold gas no longer contacts the target plate. And due to the upward airflow, there is a good synergy angle with the temperature gradient, which greatly enhances convective heat transfer (manifested as an increase in S_t). When H is higher than the flame height, even if the temperature and velocity near the target plate starts to decrease, there is a better synergy angle β. As a result, S_t continues to slowly increase before starting to gradually decrease. Therefore, it can be concluded that for optimal convective heat transfer (for maximum Q_s), H needs to be maintained at slightly higher than the flame height. Based on the above analysis, from the perspective of Q_Φ and Q_s, the optimal heat transfer effect occurs when the target plate is located approximately 2/3 of the flame cone height.

After hydrogen and oxygen enrichment (BH_{30} and BO_{30}), the LBV of the low calorific value gas BG_{30} increases from 3.9cm/s to 18.5cm/s (equivalent to BG_{60}) at φ =1.2, as shown in Fig. 8. The higher the LBV, the lower the flame height. Therefore, the flame height of BG_{30} after hydrogen enrichment and oxygen enrichment is greatly reduced. Considering the significant contribution of Q_Φ for total heat transfer from impinging flame, it is beneficial to change the shape of the target plate to optimize the heat transfer by both convection (Q_s) and heat generation in the boundary layer (Q_Φ). A case study was therefore performed to study the effect of the shape of the target plate on the total heat transfer.

Fig. 15(a) depicts the values of Q_Φ and Q_s for two cases, aiming to compare the optimal heat transfer effects at varying flame heights. Cases (I) and (II) employed BG_{30} premixed flames with hydrogen enrichments of 29% (BH_{30}) and 40%, respectively. To maintain equivalent chemical energy input in both cases, adjustments were made to the volumetric flow rate for Case (II). The increased percentage of hydrogen in the fuel mixture leads to a higher LBV in Case (II), resulting in a reduction in flame height. The Case (I) was previously discussed in Fig. 11, where H=15mm was identified as the optimal heat transfer distance (~ 2/3 of the flame cone height). However, under identical chemical energy input conditions, Case (II) exhibited a superior overall heat transfer rate. The heat transfer rate improvement is mainly due to the significant increment of convective heat transfer (Q_s). The closer proximity of the target plate to the nozzle in Case (II) intensified the impact of gas flow on the target plate leading to this increment in Q_s.

Fig. 15(b) presents the values of Q_Φ and Q_s for three cases, aiming to compare the overall heat transfer rates under different nozzle-to-plate distances and target plate shapes. Cases (I) and (III) represent the optimal overall heat transfer rate and optimal Q_s cases, respectively. As shown before, when H is slightly higher than the flame height, Q_s is optimal. By amalgamating the advantages of Cases (I) and (III), Case (IV) was formulated. The target plate used in Case (I) has been modified by introducing a cap-shape with a maximum height of H=25mm at the central axis of the flame. This strategic adjustment aimed to achieve a Q_s level equivalent to that of Case (III) while maintaining the Q_Φ value observed in Case (I). In the refined Case (IV), Q_Φ decreased from 57.11W to 11.52W. However, Q_s exhibited a noticeable increment from 106.6W to 168.1W, surpassing even the 148.3W value of Case (III). The overall heat transfer rate increased from 163.71W to 179.62W, significantly bolstering heat transfer efficiency. The superior performance of the enhanced Q_s in Case (IV), compared to Case (III) can be attributed to the cap-shape design of the target plate, enabling repeated impact of high-temperature post-combustion gases on the target plate, as illustrated in Fig. 15. When low calorific value gaseous fuels such as LCV landfill gas are used for heating applications, it is important to design the target heating plates carefully to enhance the heat transfer to extract limited chemical energy available in the gas mixtures efficiently.

5. Conclusion

In this study, heat transfer characteristics of BG_{30} under hydrogen-enrichment and oxygen-enrichment were investigated numerically. Simulations were performed with ANSYS Chemkin-pro and Fluent with GRI-Mech 3.0 mechanism. The numerical validations conducted demonstrate a strong agreement between the obtained results and the experimental data documented in the literature. The results show that the heat transfer characteristics of BG_{30} can be enhanced effectively through hydrogen and oxygen enrichment techniques. Heat transfer analysis performed using field synergy principle showed that it is important to properly design the nozzle-to-plate distance and the shape of the target plate of the combustion system to enhance the heat transfer efficiency and utilize the available limited chemical energy of low calorific value gas mixtures. The major conclusions of the study are as follows:

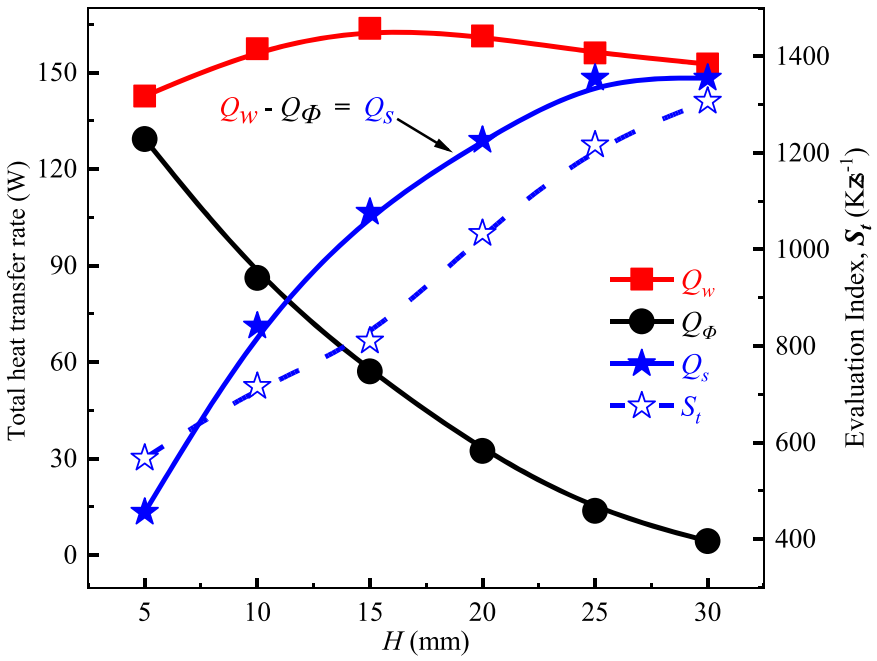

(a) BH_{30}

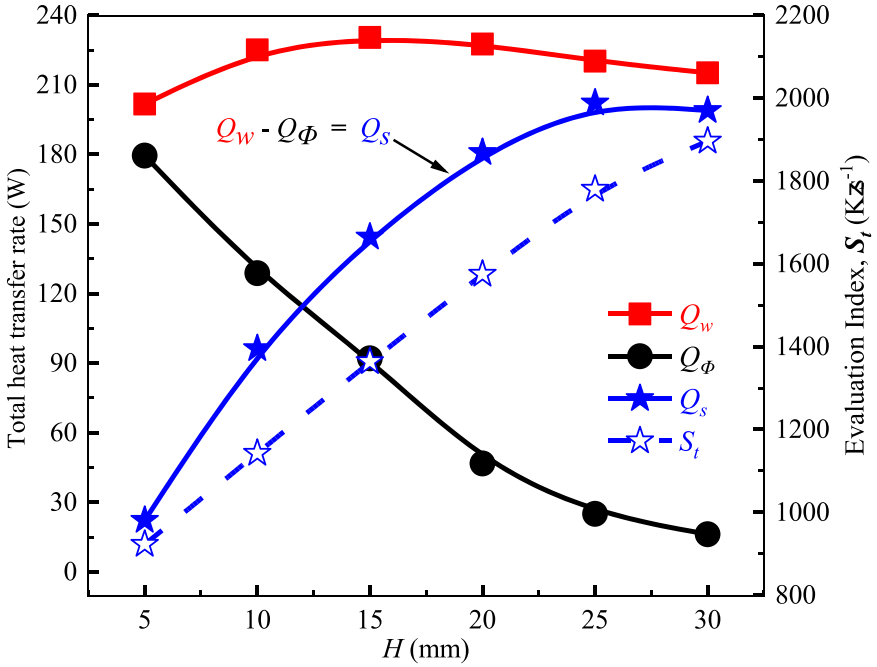

(b) BO_{30}

Fig. 13. Comparison of the variations in Q_w, Q_s, Q_Φ and S_t at different nozzle-to-plate distances (φ = 1.2).

1. In this research study, field synergy principle was used to analyze the impinging heat transfer from heat generation in the boundary layer (Q_Φ) and the convective heat transfer (Q_s). It is found that the evaluation index (S_t) provides a reliable assessment of the Q_s in the heat transfer of impinging flame.
2. The optimal distance for achieving efficient Q_s is attained when the target plate is positioned slightly higher than the tip of the flame cone.
3. Considering total heat transfer from heat generation at the boundary layer (Q_Φ) and convective heat transfer (Q_s), the optimum heat transfer occurs when the nozzle-to-plate distance is maintained at approximately 2/3 the height of the flame cone.
4. The analysis performed based on the insight obtained from field synergy principle showed that the design of a cap-shaped target plate effectively enhanced the convective heat transfer (Q_s) and hence

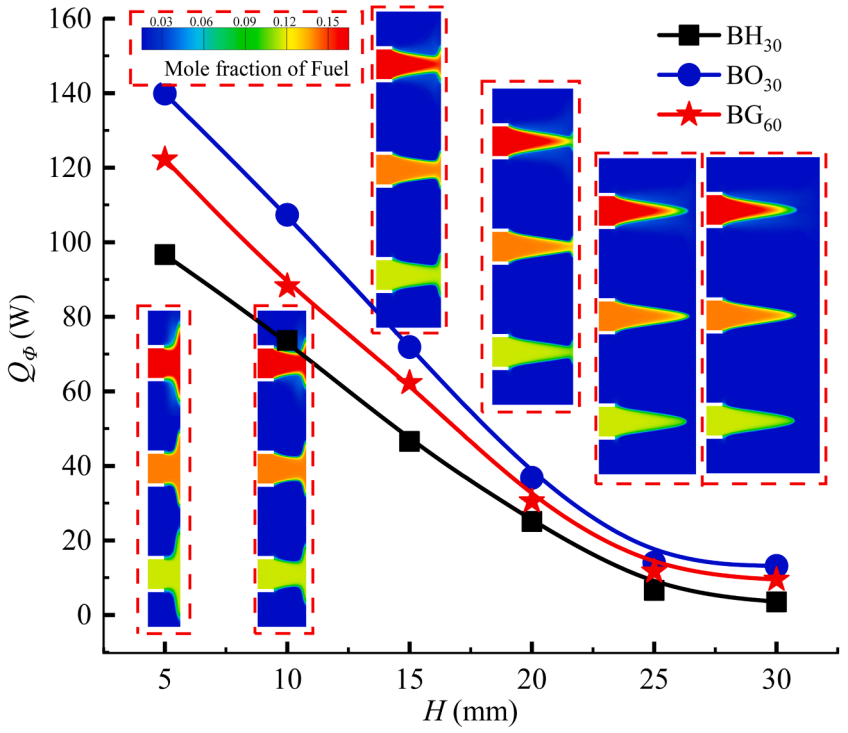

(a) Heat generated in the boundary layer, $Q\Phi$

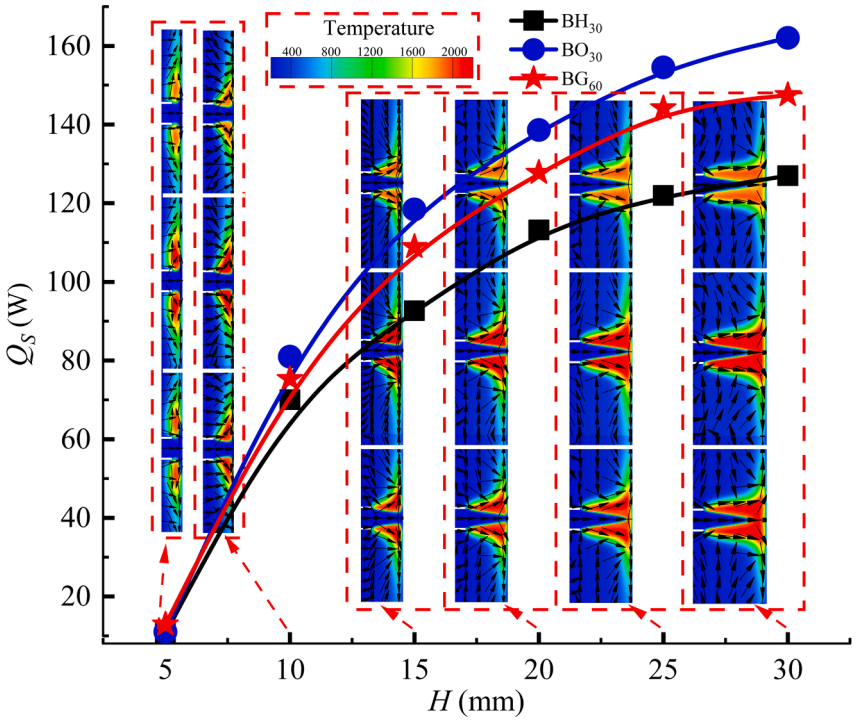

(b) Convective heat transfer, Q_S

Fig. 14. Comparison of the variations of Q_Φ and Q_s in BH_{30}, BO_{30} and BG_{60} impinging flames at different nozzle-to-plate distances at φ =1.2 (flame images correspond to the BH_{30}, BO_{30} and BG_{60}-fuels in order from top to bottom).

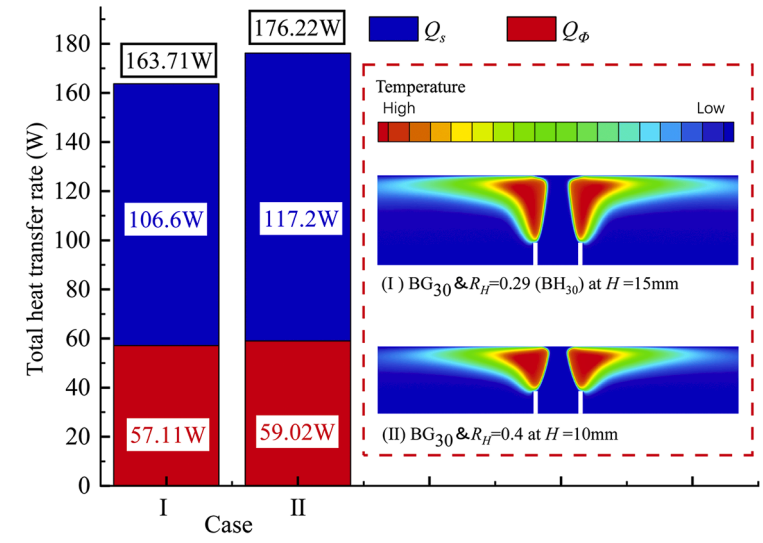

(a) Total heat transfer rates when the nozzle-to-plate distance at 2/3 of flame cone height

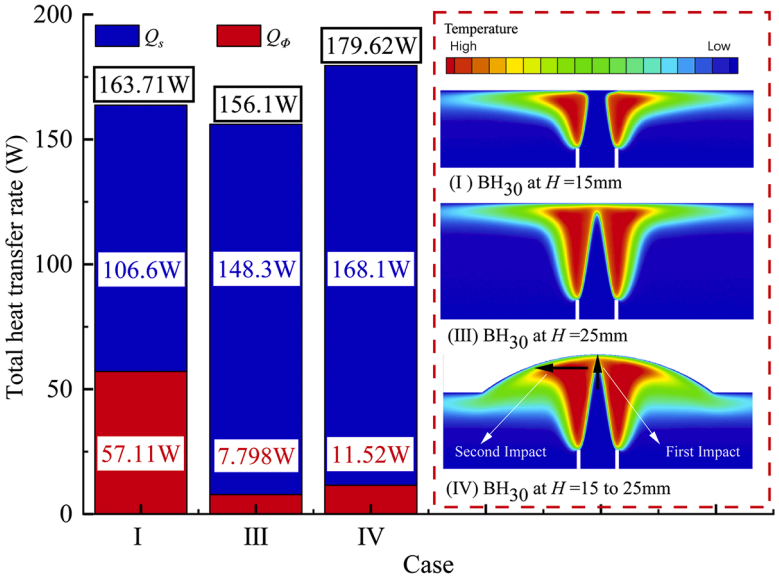

(b) Variation of total heat transfer rate with nozzle-toplate distance and shape of the target plate

Fig. 15. Comparison of the total heat transfer rates and structures of impinging flames.

total heat transfer (Q_w), as it enables the high-temperature gas flow to impinge on the target plate repeatedly.

It can be noted that a short nozzle-to-plate distance (H) can suppress the flame, causing incomplete combustion and more emissions. Conversely, a larger distance may increase free flame temperature, raising thermal NO_x levels. An optimal distance could help reduce emissions. A cap-shaped target plate can retain reactants, potentially facilitating CO to CO_2 conversion, releasing more heat and lowering undesirable emissions. Therefore, further investigation is required to assess the impact of nozzle-to-plate distance and the shape of the target plate on the formation of emissions.

CRediT authorship contribution statement

Kangdong Chen: Writing – original draft, Visualization, Validation, Software, Investigation, Formal analysis, Data curation. **Udaya Kahangamage:** Writing – review & editing, Supervision, Project administration, Methodology, Funding acquisition, Formal analysis, Conceptualization. **Kang Tan:** Investigation, Formal analysis. **Chun-wah Leung:** Writing – review & editing, Resources.

Declaration of competing interest

The authors declare that they have no known competing financial interests or personal relationships that could have appeared to influence the work reported in this paper.

Acknowledgement

The work described in this paper was fully supported by a grant from the Research Grants Council of the Hong Kong Special Administrative Region, China (UGC/FDS24/E11/22).

Data availability

Data will be made available on request.

References

[1] K. Machaj, et al., Ammonia as a potential marine fuel: A review, Energy Strategy Reviews 44 (2022), https://doi.org/10.1016/j.esr.2022.100926.

[2] A. Vandel, J.P. Chica Cano, S. de Persis, G. Cabot, Study of the influence of water vapour and carbon dioxide dilution on pollutants emitted by swirled methane/oxygen-enriched air flames, Exp. Therm. Fluid. Sci. 130 (2022), https://doi.org/10.1016/j.expthermflusci.2021.110483.

[3] Z. Fu, H. Gao, Z. Zeng, J. Liu, Q. Zhu, Generation characteristics of thermal NOx in a double-swirler annular combustor under various inlet conditions, Energy 200 (2020), https://doi.org/10.1016/j.energy.2020.117487.

[4] S. Erne, G. Scheger, W. Wiedemair, Numerical and experimental investigation of surface-stabilized combustion in a gas-fired condensing boiler, Results. Eng. 17 (2023), https://doi.org/10.1016/j.rineng.2022.100738.

[5] F. Qiu, Z. Sun, H. Li, Q. Qian, Process simulation and multi-aspect analysis of methanol production through blast furnace gas and landfill gas, Energy 285 (2023), https://doi.org/10.1016/j.energy.2023.128609.

[6] M.A. Ijaz Malik, M.A. Mujtaba, M.A. Kalam, A.S. Silitonga, A. Ikram, Recent advances in hydrogen supplementation to promote biomass fuels for reducing greenhouse gases, Int J Hydrogen Energ 49 (2024) 463–487, https://doi.org/10.1016/j.ijhydene.2023.09.154.

[7] H.M. Omar, S. Rohani, Removal of CO 2 from landfill gas with landfill leachate using absorption process, International Journal of Greenhouse Gas Control 58 (2017) 159–168, https://doi.org/10.1016/j.psep.2024.04.022.

[8] R. Paulauskas, R. Skvorčinskienė, K. Zakarauskas, N. Striūgas, Combustion performance of low calorific gas enriched by oxygen and ozone, Fuel 324 (2022), https://doi.org/10.1016/j.fuel.2022.124761.

[9] U. Kahangamage, K. Chen, H. Zhen, C.-w. Leung, Numerical investigation of combustion characteristics of hydrogen-enriched low calorific value landfill gas for energy applications, Energy Reports 12 (2024) 173–186, https://doi.org/10.1016/j.egyr.2024.06.008, 2024/12/01/.

[10] S. Molina, S. Ruiz, J. Gomez-Soriano, M. Olcina-Girona, Impact of hydrogen substitution for stable lean operation on spark ignition engines fueled by compressed natural gas, Results. Eng. 17 (2023), https://doi.org/10.1016/j.rineng.2022.100799.

[11] T. Hai, et al., A novel trigeneration model using landfill gas upgrading process and waste heat recovery: Application of methanol, desalinated water, and oxygen production, J. Clean. Prod. 393 (2023), https://doi.org/10.1016/j.jclepro.2023.136224.

[12] J. Ciuła, et al., Energy production from landfill gas, emissions and pollution indicators–Opportunities and barriers to implementing circular economy, Energy 308 (2024), https://doi.org/10.1016/j.energy.2024.132951.

[13] J.F. Fan, W.K. Ding, Y.L. He, W.Q. Tao, Three-Dimensional Numerical Study of Fluid and Heat Transfer Characteristics of Dimpled Fin Surfaces," (in English), Numer Heat Tr a-Appl 62 (4) (2012) 271–294, https://doi.org/10.1080/10407782.2012.666931.

[14] Z.Y. Guo, D.Y. Li, B.X. Wang, A novel concept for convective heat transfer enhancement, Int. J. Heat. Mass Transf. 41 (14) (1998) 2221–2225, https://doi.org/10.1016/S0017-9310(97)00272-X.

[15] Z.Y. Guo, W.Q. Tao, R.K. Shah, The field synergy (coordination) principle and its applications in enhancing single phase convective heat transfer, Int J Heat Mass Tran 48 (9) (2004), https://doi.org/10.1016/j.ijheatmasstransfer.2004.11.007.

[16] J. E, et al., Investigation on the combustion performance enhancement of the premixed methane/air in a two-step micro combustor, Appl. Therm. Eng. 141 (2018) 114–125, https://doi.org/10.1016/j.applthermaleng.2018.05.101.

[17] E. Jiaqiang, et al., Performance enhancement of microwave assisted regeneration in a wall-flow diesel particulate filter based on field synergy theory, Energy 169 (2019) 719–729, https://doi.org/10.1016/j.energy.2018.12.086.

[18] Y. Bao, H. Du, W.S. Chai, D. Nie, L. Zhou, Numerical investigation and optimization on laminar burning velocity of ammonia-based fuels based on GRI3.0 mechanism, Fuel 318 (2022), https://doi.org/10.1016/j.fuel.2022.123681.

[19] Z. Fu, et al., Investigation on effects of hydrogen addition to the thermal performance of a traditional counter-flow combustor, Energy 262 (2023), https://doi.org/10.1016/j.energy.2022.125465.

[20] Y. Tan, J. E, J. Chen, G. Liao, F. Zhang, J. Li, Investigation on combustion characteristics and thermal performance of a three rearward-step structure micro combustor fueled by premixed hydrogen/air, Renew Energ 186 (2022) 486–504, https://doi.org/10.1016/j.renene.2022.01.019.

[21] H. Liu, Z. Zeng, K. Guo, Numerical analysis on hydrogen swirl combustion and flow characteristics of a micro gas turbine combustor with axial air/fuel staged technology, Appl. Therm. Eng. 219 (2023), https://doi.org/10.1016/j.applthermaleng.2022.119460.

[22] H.S. Zhen, K.D. Chen, Z.B. Chen, Z.L. Wei, L.R. Fu, Heat transfer analysis of impinging flames using field synergy principle, Case Studies in Thermal Engineering 43 (2023) 102807, https://doi.org/10.1016/j.csite.2023.102807, 2023/03/01/.

[23] Z. Wei, H. Liu, Z. Chen, Z. Liu, H. Zhen, Quenching distance, wall heat flux and CO/NO thermochemical states in the wall vicinity of laminar premixed biogas-hydrogen impinging flame, Fuel 307 (2022), https://doi.org/10.1016/j.fuel.2021.121849.

[24] V.C. Raj, P. Kuntikana, S. Sreedhara, S.V. Prabhu, Heat transfer characteristics of impinging methane diffusion and partially premixed flames, Int J Heat Mass Tran 129 (2019) 873–893, https://doi.org/10.1016/j.ijheatmasstransfer.2018.10.009.

[25] S. Lee, O.C. Kwon, Effects of ammonia substitution on extinction limits and structure of counterflow nonpremixed hydrogen/air flames, Int. J. Hydrogen. Energy 36 (16) (2011) 10117–10128.

[26] M. Liang, Y. He, S. Liao, X. Jian, Y. Shao, Coupling effects of hydrogen transport and reactivity on NO production in laminar nonpremixed methane/air flames, Fuel 288 (2021), https://doi.org/10.1016/j.fuel.2020.119725.

[27] Z.Y. Guo, D.Y. Li, B.X. Wang, A novel concept for convective heat transfer enhancement, Int J Heat Mass Tran 41 (14) (1998), https://doi.org/10.1016/S0017-9310(97)00272-X.

[28] LIU Wei, L. ZhiChun, G. ZengYuan, Physical quantity synergy in the field of turbulent heat transfer and its analysis for heat transfer enhancement, Chinese Sci Bull 55 (23) (2010) 2592–2600, https://doi.org/10.1007/s11434-010-3009-7.

[29] V. Kumar Yadav, A. Ray, M.R. Ravi, Experimental and computational investigation of the laminar burning velocity of hydrogen-enriched biogas, Fuel 235 (2019) 810–821, https://doi.org/10.1016/j.fuel.2018.08.068.

[30] H.S. Zhen, C.W. Leung, C.S. Cheung, A comparison of the heat transfer behaviors of biogas-H-2 diffusion and premixed flames," (in English), Int. J. Hydrogen. Energy 39 (2) (Jan 13 2014) 1137–1144, https://doi.org/10.1016/j.ijhydene.2013.10.100.

[31] C. Shin, Y. Oh, S. Lee, Combustion characteristics of coaxial nonpremixed flames for low heating value gases, Energy 165 (2018) 41–52, https://doi.org/10.1016/j.energy.2018.09.096.

[32] H.S. Zhen, Z.L. Wei, Z.B. Chen, M.W. Xiao, L.R. Fu, Z.H. Huang, An experimental comparative study of the stabilization mechanism of biogas-hydrogen diffusion flame, Int. J. Hydrogen. Energy 44 (3) (2019) 1988–1997, https://doi.org/10.1016/j.ijhydene.2018.11.171, 2019/01/15/.